

# HURRICANE WIND FIELD MODEL FOR USE IN HURRICANE SIMULATIONS

By P. J. Vickery,<sup>1</sup> P. F. Skerlj,<sup>2</sup> A. C. Steckley,<sup>3</sup> and L. A. Twisdale<sup>4</sup>

**ABSTRACT:** A critical component in the simulation of hurricanes is a good representation of the hurricane wind field when given information of the storm intensity, size, and translation speed. In the investigation described here, the full nonlinear solution to the equations of motion of a hurricane are solved and then parameterized for use in fast-running simulations. The hurricane model described here takes into account the effects of changing sea surface roughness and the air-sea temperature difference on the estimated surface-level wind speeds. Comparisons between modeled and observed hurricane wind speed records are performed where one compares both the 10-min mean wind speeds and the peak gust wind speeds. The resulting wind field model represents the most physically based and validated model used in the estimate of hurricane wind speed exceedance probabilities.

## INTRODUCTION

The modeling of the hurricane wind field is a key component in the hurricane simulation process. A new wind field model for use in the simulation of hurricanes is described here that draws on the work of Chow (1971) and Thompson and Cardone (1996). The model is an improvement over the Shapiro-based numerical model used by Georgiou (1985) and Vickery and Twisdale (1995a) in that the asymmetries in fast-moving hurricanes are more accurately modeled, the effect of the sea surface roughness is properly modeled, and a physically based boundary layer model is used. The wind field model is based on the full nonlinear solution of the equations of motion of a translating hurricane. The hurricane wind field is coupled with a parameterized hurricane boundary layer model that accounts for the effects of the sea surface roughness and the air-sea temperature difference. The wind field model draws on individual model components developed over the past 2 decades by a number of researchers and organizations. Over 90 full-scale hurricane wind speed measurements are used to evaluate the validity of the hurricane wind field model. The resulting model is believed to be a significant improvement over other wind models used in hurricane risk studies.

## WIND FIELD MODELING

The hurricane wind field model used herein is based on a dynamic numerical model of the planetary boundary layer (PBL). The model considers the equation of horizontal motion, vertically averaged over the height of the PBL. A finite-difference scheme is used to solve for the steady-state wind field over a set of nested rectangular grids. The basis of this approach is the assumption that the large-scale structure of the hurricane wind fields changes relatively slowly over time. Therefore, at any instant the wind field may be considered to be very nearly at steady-state conditions. The finite-difference

model is used to develop several thousand wind fields for a wide range of input parameters. These wind fields are then fit using a Fourier fitting approach so that each wind field can be described using relatively few parameters.

## Finite-Difference Model

The model is based on a formulation developed by Chow (1971) and is similar to the model given in Thompson and Cardone (1996) but is simplified for use in Monte Carlo simulations. The equation of horizontal motion, vertically averaged through the height of the PBL, is written in earth fixed coordinates

$$\frac{d\mathbf{V}}{dt} + f|\mathbf{k} \times \mathbf{V}| = -\frac{1}{\rho} \nabla p + \nabla \cdot (K_H \nabla \mathbf{V}) - \frac{C_D}{h} |\mathbf{V}| \mathbf{V} \quad (1a)$$

where

$$\frac{d}{dt} = \frac{\partial}{\partial t} + \mathbf{V} \cdot \nabla \quad (1b)$$

Here  $\mathbf{V}$  = vertically averaged horizontal velocity;  $f$  = Coriolis parameter;  $\mathbf{k}$  = unit vector in the vertical direction;  $\rho$  = air density;  $p$  = atmospheric pressure;  $K_H$  = horizontal eddy viscosity coefficient;  $C_D$  = drag coefficient; and  $h$  = height of the PBL.

This equation is first transformed to a moving coordinate system with Cartesian coordinates  $(x, y)$  whose origin is located at the storm center. One is then interested in determining the wind field denoted by  $\mathbf{V}_s = \mathbf{V} - \mathbf{V}_c$ , where  $\mathbf{V}_c$  is the translational velocity of the storm. Eq. (1) becomes

$$\frac{d\mathbf{V}}{dt} + f|\mathbf{k} \times \mathbf{V}_s| = -\frac{1}{\rho} \nabla p + \nabla \cdot (K_H \nabla \mathbf{V}_s) - \frac{C_D}{h} |\mathbf{V}_s + \mathbf{V}_c| (\mathbf{V}_s + \mathbf{V}_c) \quad (2a)$$

where

$$\frac{d}{dt} = \frac{\partial}{\partial t} + (\mathbf{V}_s + \mathbf{V}_c) \cdot \nabla \quad (2b)$$

One may simplify (2) using the following notation:

$$\frac{d\mathbf{V}_s}{dt} = \mathbf{F} + \mathbf{P} + \mathbf{E} + \mathbf{D} \quad (3)$$

where  $\mathbf{F}$ ,  $\mathbf{P}$ ,  $\mathbf{E}$ , and  $\mathbf{D}$  = accelerations induced by the Coriolis forces, pressure gradient, fluid viscosity, and surface drag forces, respectively. Hence

<sup>1</sup>Sr. Engr., Applied Research Associates, 811 Spring Forest Rd., Ste. 100, Raleigh, NC 27609.

<sup>2</sup>Staff Engr., Applied Research Associates, 811 Spring Forest Rd., Ste. 100, Raleigh, NC.

<sup>3</sup>Sr. Engr., Applied Research Associates, 811 Spring Forest Rd., Ste. 100, Raleigh, NC.

<sup>4</sup>Prin. Engr., Applied Research Associates, 811 Spring Forest Rd., Ste. 100, Raleigh, NC.

Note. Associate Editor: Timothy A. Reinhold. Discussion open until March 1, 2001. Separate discussions should be submitted for the individual papers in this symposium. To extend the closing date one month, a written request must be filed with the ASCE Manager of Journals. The manuscript for this paper was submitted for review and possible publication on January 26, 1998. This paper is part of the *Journal of Structural Engineering*, Vol. 126, No. 10, October, 2000. ©ASCE, ISSN 0733-9445/00/0010-1203-1221/\$8.00 + \$.50 per page. Paper No. 17442.

$$\mathbf{F} = -f|\mathbf{k} + \mathbf{V}_s| \quad (4)$$

$$\mathbf{P} = -\frac{1}{\rho} \nabla p \quad (5)$$

$$\mathbf{E} = \nabla \cdot (K_H \nabla \mathbf{V}_s) \quad (6)$$

$$\mathbf{D} = -\frac{C_D}{h} |\mathbf{V}_s + \mathbf{V}_c| (\mathbf{V}_s + \mathbf{V}_c) \quad (7)$$

Denoting the components of  $\mathbf{V}_s$  as  $u$  and  $v$ , one may derive from (3) the following expressions for the acceleration components:

$$\frac{\partial u}{\partial t} = -A_u + F_u + P_u + E_u + D_u \quad (8a)$$

$$\frac{\partial v}{\partial t} = -A_v + F_v + P_v + E_v + D_v \quad (8b)$$

where  $A_u$  and  $A_v$  = advection terms given by

$$A_u = \frac{\partial u}{\partial x} u + v \frac{\partial u}{\partial y}; \quad A_v = u \frac{\partial v}{\partial x} + v \frac{\partial v}{\partial y} \quad (9a,b)$$

The components of  $\mathbf{F}$ ,  $\mathbf{P}$ ,  $\mathbf{E}$ , and  $\mathbf{D}$  are given by

$$F_u = f v, \quad F_v = -f u \quad (10a,b)$$

$$P_u = -\frac{1}{\rho} \frac{dp}{dx}; \quad P_v = -\frac{1}{\rho} \frac{dp}{dy} \quad (11a,b)$$

$$E_u = \frac{\partial K_H}{\partial x} \frac{\partial u}{\partial x} + \frac{\partial K_H}{\partial y} \frac{\partial u}{\partial y} + K_H \left( \frac{\partial^2 u}{\partial x^2} + \frac{\partial^2 u}{\partial y^2} \right) \quad (12a)$$

$$E_v = \frac{\partial K_H}{\partial x} \frac{\partial v}{\partial x} + \frac{\partial K_H}{\partial y} \frac{\partial v}{\partial y} + K_H \left( \frac{\partial^2 v}{\partial x^2} + \frac{\partial^2 v}{\partial y^2} \right) \quad (12b)$$

$$D_u = \frac{C_D}{h} (u + u_c) \sqrt{(u + u_c)^2 + (v + v_c)^2} \quad (13a)$$

$$D_v = \frac{C_D}{h} (v + v_c) \sqrt{(u + u_c)^2 + (v + v_c)^2} \quad (13b)$$

where  $u_c$  and  $v_c$  = components of the storm translation vector  $\mathbf{V}_c$ .

The horizontal eddy viscosity coefficient is given after Smagorinsky (1963)

$$K_H = 2\kappa^2 \left( \frac{\Delta x}{2} \right)^2 \sqrt{\left( \frac{\partial u}{\partial x} \frac{\partial v}{\partial y} \right)^2 + \left( \frac{\partial v}{\partial x} \frac{\partial u}{\partial y} \right)^2} \quad (14)$$

where  $\kappa$  = nondimensional proportionality constant taken to be 0.4 (Chow 1971; Thompson and Cardone 1996). A sensitivity study that varied  $\kappa$  by  $\pm 50\%$  shows that the influence of the horizontal eddy viscosity coefficient on the modeled hurricane wind speed estimates is negligible.

With these equations, inputs to the model are the pressure gradients ( $dp/dx$  and  $dp/dy$ ), the surface drag coefficient  $C_D$ , the latitude of the storm (from which  $f$  is derived), and the storm's translational velocity ( $u_c$  and  $v_c$ ). The pressure gradients and surface drag coefficient may be arbitrarily defined at each node point over the region of the finite-difference grid. In the over water case, the drag coefficient is modeled using the same model given in Vickery and Twisdale (1995a). In the over land case, the drag coefficient is modeled as a constant, taking on a value of 0.005. The PBL height is taken as 1 km in all cases.

The pressure gradients  $dp/dx$  and  $dp/dy$  are prescribed by transforming the following expression for the radial pressure gradient:

$$\frac{\partial p}{\partial r} = \frac{\Delta p B}{r} \left( \frac{R_{\max}}{r} \right)^B \exp \left( - \left( \frac{R_{\max}}{r} \right)^B \right) \quad (15)$$

where  $B$  = Holland's radial pressure profile parameter (Holland 1980), taking on values between 0.5 and 2.5 (Thompson and Cardone 1996);  $\Delta p$  = central pressure deficit;  $R_{\max}$  = radius to maximum winds; and  $r$  = radial distance from the storm's pressure center.

## Finite-Difference Scheme

A finite-difference scheme is used to integrate the equations of motion forward in time. An initial estimate of the wind field is defined by the gradient balance equation. The solution to the questions of motion is evolved to the steady-state wind field solution by integrating forward until the acceleration is acceptably small. To enhance numerical stability, upwind differences are used for all first-order spatial derivatives. This is particularly important for the gradients resulting from the advective terms of (9). Central differences are used for the second-order spatial differences, which occur only in the eddy viscosity terms defined in (12).

## Nested Grid

As in Thompson and Cardone (1996), a nested grid is used to solve for the steady-state wind field using the finite-difference approach. The system comprises four concentric rectangular grids. Each grid comprises the same number of nodes, but the internode distance is halved with each successive grid; hence, each covers 25% of the area of the previous grid. The outermost nodes, or boundary nodes, of the outermost grid are held fixed at values determined by solving (3) for the steady-state condition with  $\mathbf{E} = \mathbf{D} = \mathbf{0}$ . This amounts to balancing the pressure gradient and Coriolis forces. The remaining nodes of the outermost grid are then solved by integrating forward in time until the acceleration is acceptably small. The boundary nodes for the next grid are then set according to this solution, and the next grid is solved. This procedure continues until the innermost grid is solved. The results from the boundary nodes of the inner grids are then successively assigned to the appropriate node points in the common area of the next grid outward. This ensures that the final results of the four grids are in exact agreement and utilizes, at each location, the results from the finest resolution grid available. Because the velocities relative to the storm center have been calculated, the storm's translation velocity is added onto the results to get the earth-centered velocity field.

The grid size ranges from a minimum of 2 km for the smallest storms ( $R_{\max} = 8$  km) and up to 15 km for the largest storms ( $R_{\max} = 150$  km). These grid sizes correspond to overall domain sizes of  $512 \times 512$  km and  $3,840 \times 3,840$  km for the smallest and largest storms, respectively. The transition from the finest grid to the next coarser grid occurs between  $1.6R_{\max}$  and  $4R_{\max}$  from the center of the overall grid. The next grid transition occurs between  $3.2R_{\max}$  and  $8R_{\max}$  from the grid center, and the final transition occurs at a distance ranging from  $6.4R_{\max}$  to  $16R_{\max}$ .

## Fourier Fitting

To cover the full range of combinations of storm central pressure, radius to maximum winds, and translation speed expected in a full simulation, a total of 1,560 storms were simulated for each of nine different values of the Holland profile parameter ranging between 0.5 and 2.5. The storms include central pressure deficits ranging from 1 to 150 mbar, radii to maximum winds ranging from 8 to 150 km, and translation speeds ranging from 0 to 40 m/s. One complete set of hurricanes were generated for the over water case and another set

for the over land case. For each storm, cubic splines fitted along the  $x$ - and  $y$ -directions were used to interpolate  $u$  and  $v$  components at points around circular paths concentric with the grid center. These were then transformed to a Fourier series in the form

$$u(r_j) = u_0(r_j) + \sum_{i=1}^N u_{c_i}(r_j)\cos(i\lambda) + \sum_{i=1}^N u_{s_i}(r_j)\sin(i\lambda) \quad (16a)$$

$$v(r_j) = v_0(r_j) + \sum_{i=1}^N v_{c_i}(r_j)\cos(i\lambda) + \sum_{i=1}^N v_{s_i}(r_j)\sin(i\lambda) \quad (16b)$$

where  $r_j$  takes on values at increments equal to the smallest grid size. The number of terms  $N$  used in the expansion to describe the wind field is 4 for storms translating at speeds <16 m/s and 8 for storms translating at speeds of >16 m/s. A larger number of terms is used for the faster moving storms, as these storms are more asymmetric than the slower moving storms. The Fourier coefficients,  $u_0(r_j)$ ,  $u_{c_i}(r_j)$ ,  $u_{s_i}(r_j)$ ,  $v_0(r_j)$ ,  $v_{c_i}(r_j)$ , and  $v_{s_i}(r_j)$ , are stored and recalled as needed for simulating a given storm. For each simulated storm, the velocities  $u$  and  $v$  are found through a combination of interpolation and scaling from the results stored on disk. A quadratic interpolation technique is used to interpolate in the  $V_c$  and  $\Delta p$  space, and a scaling procedure is used to interpolate between different values of  $R_{\max}$ . Linear interpolation is used elsewhere.

A similar approach for modeling hurricane wind fields resulting from a numerical solution to the equations of motion for a translating hurricane was first used by Georgiou (1985) and then by Vickery and Twisdale (1995a). In both of these studies, the numerical model results were obtained from Shapiro's model (1983), where the solutions to the equations of motion were themselves solved using a spectral approach employing the first two terms of the expansion. The approach used here has an advantage over the use of the Shapiro model in that the full nonlinear equations are solved and then the results are fit to a Fourier series using more than two terms, hence maintaining a more precise solution to the equations of motion. This will be discussed in more detail later in the report.

## Boundary Layer Modeling

In all hurricane simulation procedures published to date, including Russell (1971), Batts et al. (1980), Georgiou et al. (1983), Georgiou (1985), and Vickery and Twisdale (1995a), the hurricane boundary layer was defined using empirical relationships between the upper-level winds and the surface-level (10-m) winds. The ratio of the surface-level winds to the upper-level winds within these empirical models is very high (0.8–0.9) compared to typical values in extratropical storms (ratio of about 0.6 in open country terrain). As described in Powell (1980), Powell and Black (1990), and Thompson and Cardone (1996), the ratio of the surface-level winds to the upper-level winds within the hurricane is primarily a function of the air-sea temperature difference and the sea surface roughness, which is itself a function of wind speed. This investigation uses a more theoretically based model of the hurricane boundary layer, as described by Arya (1988). The resulting boundary layer model is similar to that used by Thompson and Cardone (1996) and yields ratios of the surface-level wind speeds (at 10 m) to the gradient-level wind speeds, which vary as a function of the air-sea temperature difference and the mean wind speed at the surface.

The modeled ratios between the surface and integrated wind speed resulting from the boundary layer model are plotted in Fig. 1 for the unstable cases (sea temperature greater than air temperature) and the neutral case. The ratios decrease with increasing mean wind speed for a given air-sea temperature

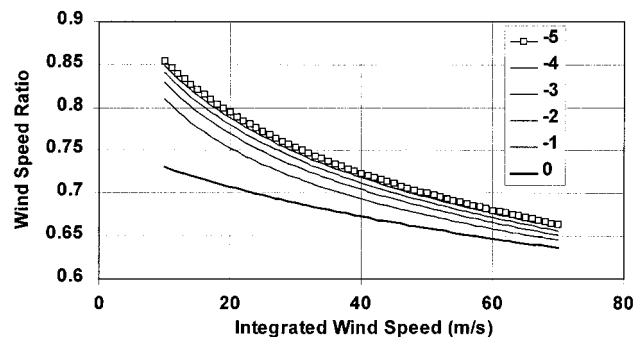


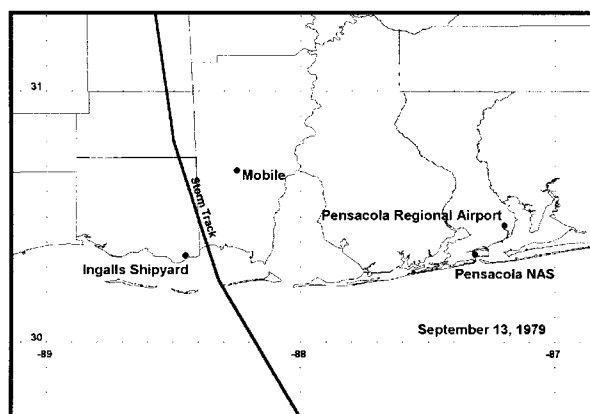
FIG. 1. Ratio of Surface-Level Mean Wind Speed to Integrated Mean Wind Speed as Function of Air-Sea Temperature Difference

difference because the surface roughness increases over water with increasing wind speed, which leads to a reduction in the surface-level wind speeds but has no influence on the upper-level wind speeds. In the stable boundary layer case, the neutral boundary layer model is used. This will generally lead to conservative wind speed estimates for regions north of the North Carolina/Virginia border, where stable conditions typically apply because the water temperatures decrease as the Gulf Stream moves east away from the coast. However, the wind speed comparisons for Hurricane Bob at the marine stations located north of 38° (Fig. 2) do not show this bias. As in Vickery and Twisdale (1995a) and Thompson and Cardone (1996), the surface-level wind speeds resulting from the model are assumed to be representative of 1-h mean values.

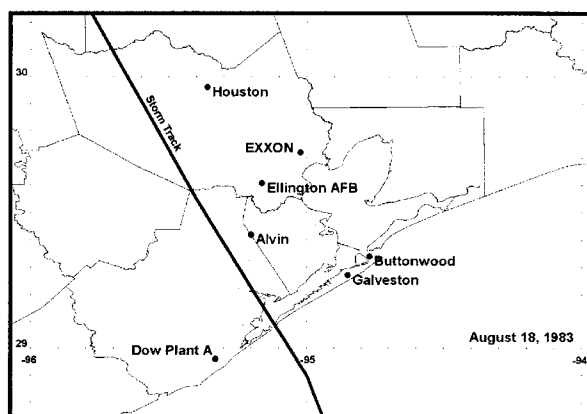
## Empirical Adjustments and Land-Sea Interface Modeling

After performing some preliminary comparisons between simulated and observed hurricane wind speeds, the boundary layer model was modified in the eye-wall region. The empirical modification increases the ratio of the mean surface-level winds to the upper-level winds by 10% for  $r \leq R_{\max}$  with a smooth cosine transition to no increase at  $r = 2R_{\max}$ . The nature of the boundary layer within the eye wall of the hurricane is still a controversial subject, and this modification is consistent with the higher ratios between surface-level and upper-level winds apparent in most of the empirical hurricane boundary layer models and in hurricane rain bands that include the eye wall. New research using dropwindsondes [e.g., Hock and Franklin (1999), and Powell et al. (1999)] to measure the velocity profiles in hurricane eye walls may shed more light on the characteristics of the eye wall boundary layer, but until this research is completed, the 10% increase used in the current model yields good estimates of hurricane wind speeds.

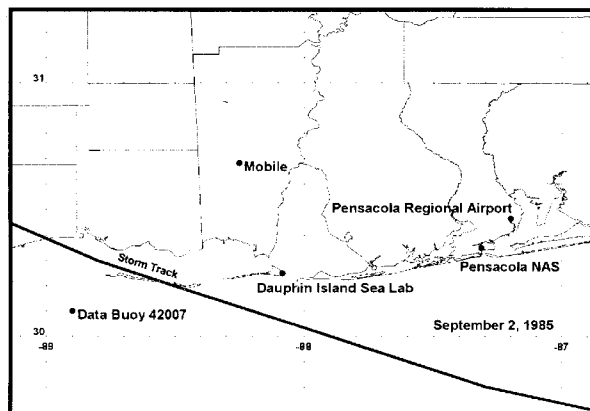
As noted above, because the hurricane wind fields are pre-computed for either the all over water case or the all over land case, a true simulation of the effects of the sea-land interface cannot be modeled for a hurricane crossing the coast without resorting to a case specific solution to the equations of motion. In the simulation process, the wind field is modeled using linear interpolation. For sites located at distances of 50 km or more from the coast, the wind field derived for the over land case is used, and for locations <10-km inland from the coast, the over water model is used. For stations located between 10 and 50 km from the coast, the wind field is computed using a weighted linear combination of the over land and over water wind fields. The chosen distances and interpolation method are based on engineering judgment. The stability effects and the 10% increase of the surface winds near the eye wall are lin-



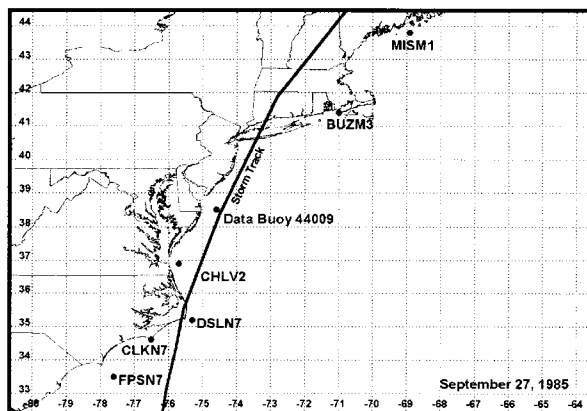
Hurricane Frederic (1979)



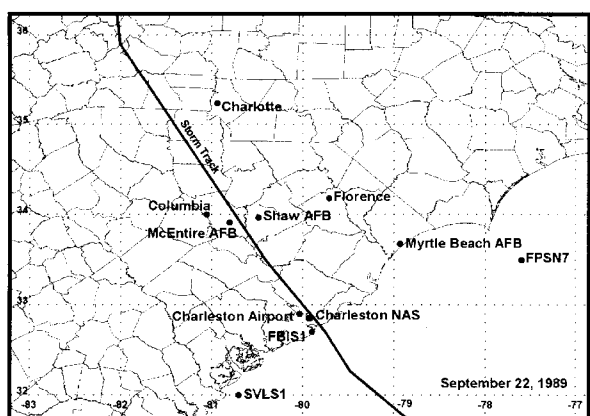
Hurricane Alicia (1983)



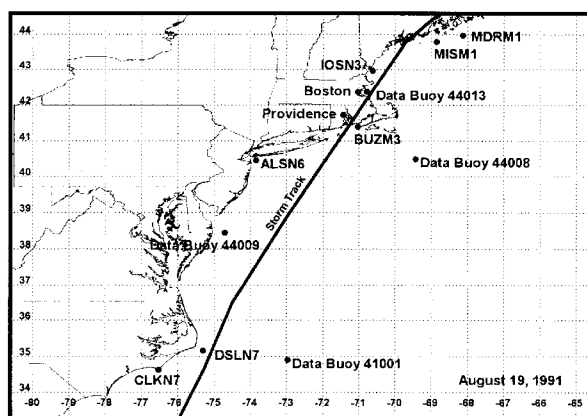
Hurricane Elena (1985)



Hurricane Gloria (1985)



Hurricane Hugo (1989)



Hurricane Bob (1991)

FIG. 2. Tracks of Hurricanes Examined Showing Location of Anemometers

early decayed from the coast to be nonexistent at a distance of 50-km inland.

In the transition of the flow from the sea to the land, an internal boundary layer develops. This boundary layer comprises three regimes. In the lowest regime, the flow is controlled by the local roughness and, in the upper regime, the flow is controlled by the upwind roughness. In the intermediate regime, the flow is not in equilibrium with either the local or upwind roughness. In Powell et al. (1996), the height associated with this outer regime is given

$$h_i = 0.1Cz_0(x/z_0)^{0.8} \quad (17)$$

where  $x$  = distance from the coast;  $h_i$  = thickness of the inner layer  $x$  from the coast; and the constant  $C$  varies between 0.28 and 0.75, depending on the stability. For a surface roughness

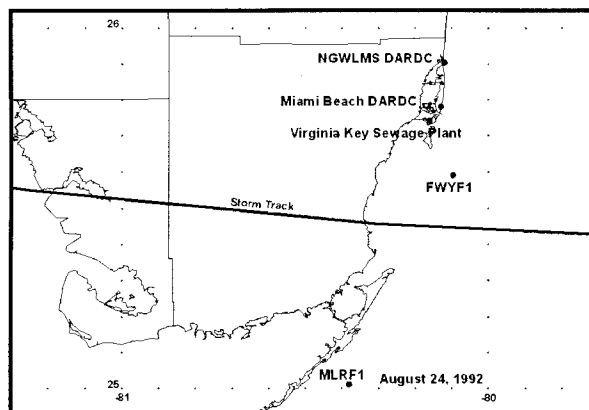
of 0.03 m, the internal boundary layer height reaches 10 m at distances ranging between 1 and 3 km from the coast, depending on the value of  $C$  chosen. Note that equilibrium with the local roughness for heights  $>10$  m is achieved at distances from the coast longer than those stated above.

Deaves (1981) presents a different model for  $h_i$

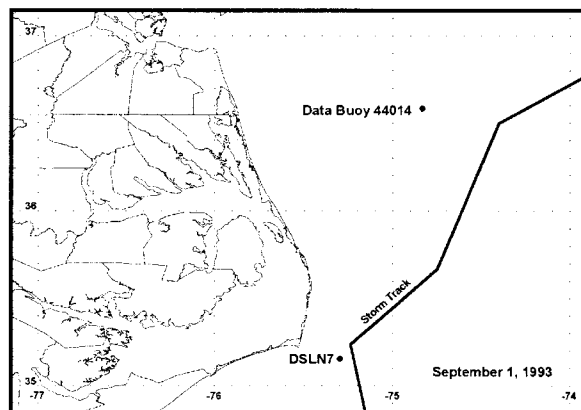
$$h_i = 0.36z_0(x/z_0)^{0.75} \quad (18)$$

In the Deaves model, equilibrium of the mean flow (for heights of 10 m and less) is reached after a distance of only about 270 m, whereas equilibrium of the RMS velocities is reached after a distance of about 3 km.

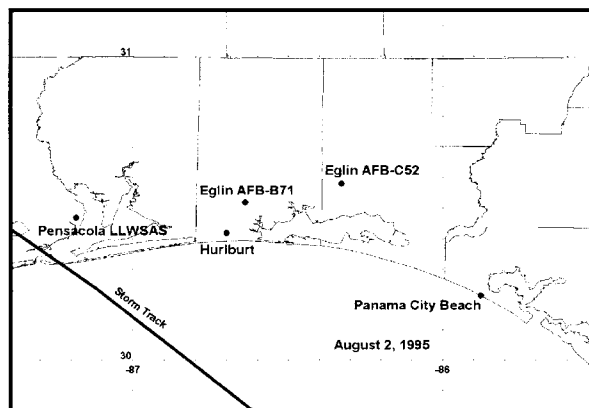
For simulation purposes, the effect of the change in the roughness length is performed using a linear reduction in wind speed taken over a 2-km distance from the coast.



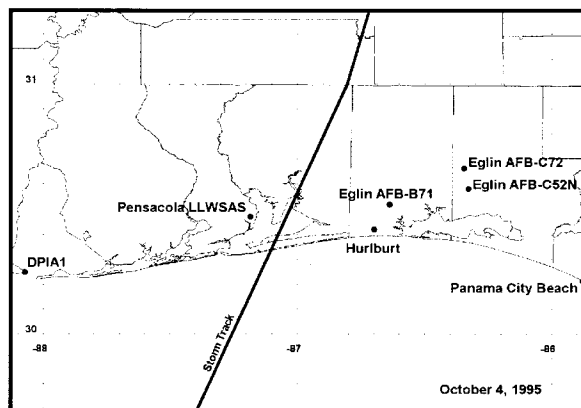
Hurricane Andrew (1992)



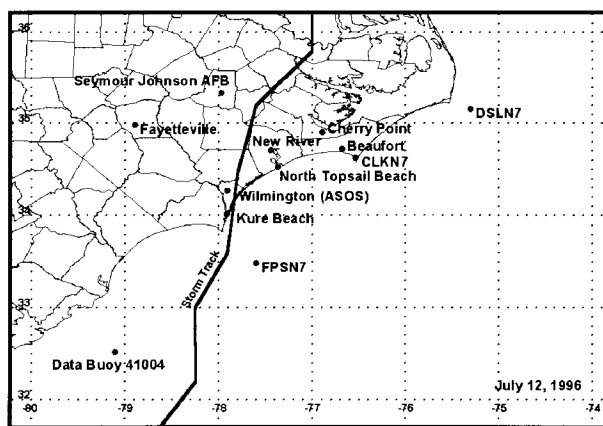
Hurricane Emily (1993)



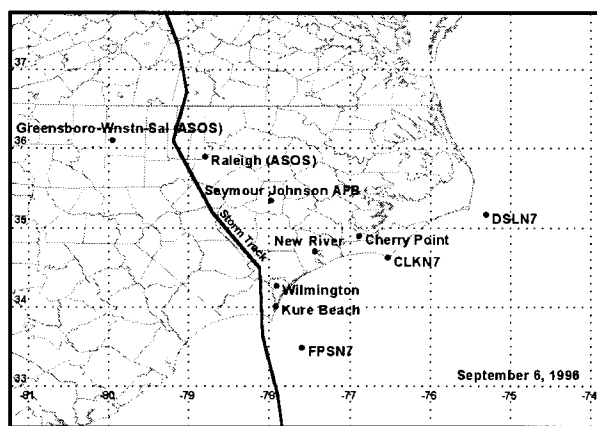
Hurricane Erin (1995)



Hurricane Opal (1995)



Hurricane Bertha (1996)



Hurricane Fran (1996)

FIG. 2. (Continued)

## HURRICANE WIND FIELD MODEL VALIDATION

Because of the assumptions, simplifications, and the empirical model components used in the development of the wind field model, evaluation of the model through comparisons with full-scale hurricane data is critical and provides the only means to assess the overall usefulness of the model. In all the comparisons given, the prime source of information on central pressure deficit, storm position, direction, and translation speed used to evaluate the wind field models was the HURDAT data base, which is described by Jarvinen et al. (1984). Information on radius to maximum winds was obtained from a number of sources in the literature, including Ho et al. (1987), Golden (1984), Willoughby (1990), Powell et al. (1991), Houston and Powell (1993), Burpee et al. (1994), Houston et al. (1997), and Powell and Houston (1998). This

information was supplemented with the upper-level aircraft data supplied by H. Willoughby of the Hurricane Research Division (HRD) of the National Oceanic and Atmospheric Administration (NOAA). Upper-level data were available for all storms that were examined prior to 1992. Information on the air-sea temperature difference was obtained from data observed at buoy or Coastal-Marine Automated Network (C-MAN) stations close to the landfall location. The effective value of the Holland profile parameter  $B$  is estimated on a storm-by-storm basis, based on comparisons between the simulated and observed peak gust and 10-min mean wind speeds. The values of  $B$  for Hurricanes Alicia, Frederic, Elena, and Bob used in the comparisons are consistent with the  $B$  values derived from the aircraft measured velocities for flights at 850-mbar surfaces (approximately 1,500-m above sea level).

**TABLE 1. Comparison of Observed and Simulated Maximum Gust Wind Speeds for Marine Stations Having Complete Continuous Records**

Hurricane and station (1)	Measured peak gust at 10 m (m/s) (2)	Anemometer height (m) (3)	Wind Speed Averaging Time (s) (4)		Holland's <i>B</i> parameter (6)	Air-sea temperature difference (°C) (7)	Radius to maximum winds (km) (8)	Simulated peak gust speed at 10 m (m/s) (9)	Simulated divided by observed (10)
			Mean (4)	Gust (5)					
Fran (1996)									
FPSN7	48.3, 37.7	44.2	600	5	0.95	0	85	47.6, 45.0	0.99, 1.19
CLKN7	37.3	9.8	600	5	0.95	0	85	36.7	0.98
DSL7	29.6	46.6	600	5	0.95	0	85	27.2	0.92
Bertha (1996)									
FPSN7	45.1	44.2	600	5	1.2	−0.5	70	46.5	1.03
CLKN7	38.6	9.8	600	5	1.2	−0.5	70–75	37.6	0.97
DSL7	35.4	46.6	600	5	1.2	−0.5	70–75	26.7	0.75
Emily (1993)									
DSL7	51.0, 56.7	46.6	600	5	1.7	0	39	59.4, 56.2	1.16, 0.99
Andrew (1992)									
MLRF1	29.9	15.8	600	5	1.6	−3	19	36.4	1.22
NGW LMS	58.6	13.7	120	5	1.6	−3	19	45.1	0.77
Bob (1991)									
DSL7	47.6	46.6	600	5	1.4	0	35	51.4	1.08
CLKN7	24.1	9.8	600	5	1.4	0	35	20.9	0.87
41001	30.6	5.0	600	5	1.4	0	35	23.6	0.77
44008	31.3	13.8	600	5	0.8	0	55–70	32.0	1.02
Hugo (1989)									
FPSN7	31.7	44.2	600	5	1.0	0	40	29.7	0.94

Tables 1 and 2 summarize the key hurricane parameters used to model each storm, in addition to the station anemometer height, estimated surface roughness (for land stations), and the maximum observed and simulated peak gust wind speed (10 m above ground, actual terrain) for each site. Fig. 2 shows the location of the anemometers with respect to the storm track. The data presented in Tables 1 and 2 include only those records that are complete and are either continuous and/or contain the maximum wind speed produced by the storm. Note that no data for Hurricane Gloria are given in Tables 1 or 2, as no continuous records were obtained for this storm. The results presented in Tables 1 and 2 do not account for any errors in the estimates of storm position, central pressure, surface roughness, gust factors, pressure profile parameter, or radius to maximum winds. Figs. 3–6 present graphical comparisons of the simulated and observed wind speeds for the examples highlighted in Tables 1 and 2. Figs. 3 and 4 also present data for the two incomplete wind speed records (FWYFI—i.e., Fowey Rocks, Fla., from Hurricane Andrew and Dauphin Island Marine Lab, Ala., from Hurricane Elena).

The wind speed data given in Figs. 3–6 present comparisons of both the 3-s peak gust and 10-min mean wind speeds at a height of 10 m. The wind speeds are representative of the site's local surface roughness. In the case of the full-scale data, two estimates of both the peak gust and the mean wind speeds are given. In the case of the peak gust speed, one estimate of the peak gust is derived from the peak gust itself (i.e., the "true" value) and the second estimate of the peak gust is derived from the mean wind speed (typically 10 min). In cases where the true peak gust speeds exceeds the peak gust speed estimated from the observed mean speed, the actual gust factor is larger than the modeled gust factor. When the true gust speed is lower than the peak gust speed estimated from the observed mean speed, the reverse is true. The two estimates of the full-scale 10-min mean wind speed are derived from the peak gust and the longer period average wind speed. All adjustments for averaging time are made using the Engineering Sciences Data Unit, London, based gust factor models ("Strong" 1982, 1983) shown to be suitable for describing the

hurricane gust structure in Vickery and Skerlj (unpublished manuscript, 2000). Note that the plotted observed speeds in Figs. 3–6 are shown with a triangle symbol when they are derived from the gust speed observation and with a circle symbol when they are derived from the mean speed observation.

Results shown in Fig. 3 are for marine stations. At all locations, except CLKN7 (Cape Lookout, N.C.), the hurricanes passed within a distance of  $1R_{\max}$  from the station. For the CLKN7 station the distance of closest approach was  $1.8R_{\max}$ . A visual comparison of the results shows generally good agreement between the simulated and observed data, except in the case of Hurricane Emily, where the model overestimates the wind speeds on the front side of the storm. In the case of Hurricanes Fran and Bertha, the simulated wind speeds at FPSN7 (Frying Pan Shoals, N.C.) agree well with the observed wind speeds on the front side of the storm, but in both cases the model overestimates the wind speeds on the back side of the storm, with the overestimate larger in the case of Hurricane Fran. An interesting feature of the Hurricane Bob comparisons at DSLN7 (Diamond Shoals, N.C.) occurs at the two peaks. The overestimate of the peak gust wind speed for the first peak corresponds to the existence of a low gust factor occurring at the time of the peak mean wind. At the second peak, the underestimate of the peak wind is coincident with the occurrence of a high gust factor. At CLKN7, the model wind speeds generally underestimate the observed wind speeds, with the difference probably attributable to a variation in  $B$  and/or  $R_{\max}$  over the domain of the storm.

Fig. 4 shows comparisons of simulated and observed wind speeds for four coastal stations (<3 km from the coast). Wind speed data from the Kure Beach, N.C., station were obtained for both Hurricanes Bertha and Fran. Hurricane Bertha passed at a distance of  $0.1R_{\max}$  to the right of the site, and Hurricane Fran passed within a distance of  $0.2R_{\max}$  to the left of the site. In the case of Hurricane Fran, the overestimate of the peak wind speed in the storm at Kure Beach arises from a low value of  $C_G$  occurring when the maximum mean wind speed was observed. In the case of Hurricane Bertha, the potential overestimate of the peak gust wind speed was lessened due to the

**TABLE 2. Comparison of Observed and Simulated Maximum Gust Wind Speeds for Land-Based Stations Having Complete Continuous Records**

Hurricane and station (1)	Measured peak gust at 10 m (m/s) (2)	$z_0$ (m) (3)	Anemometer height (m) (4)	Wind Speed Averaging Time (s)		Holland's $B$ parameter (7)	Radius to maximum winds (km) (8)	Simulated peak gust speed at 10 m (m/s) (9)	Simulated divided by observed (10)
				Mean (5)	Gust (6)				
Fran (1996)									
Kure Beach	41.7	0.02	10	3,600	3	0.95	85	46.0	1.10
Wilmington ASOS, N.C.	39.2	0.05	10	600	5	0.95	85	43.1	1.10
Raleigh ASOS, N.C. <sup>a</sup>	34.0	0.05	10	120	3	0.95	85	38.4	1.13
New River, N.C. <sup>a</sup>	41.5	0.05	10	120	3	0.95	85	42.3	1.02
Greensboro Airport, N.C. <sup>a</sup>	24.5	0.05	10	120	3	0.95	85	23.0	0.94
Cherry Point CF, N.C.	34.6	0.10	10	600	5	0.95	85	34.7	1.00
Cherry Point R32, N.C.	32.0	0.10	10	600	5	0.95	85	34.7	1.08
Seymour Johnson AFB, N.C. <sup>a</sup>	41.4	0.05	4	120	3	0.95	85	41.8	1.01
Bertha (1996)									
Kure Beach	40.5	0.02	10	3,600	3	1.2	70	41.9	1.03
Wilmington ASOS <sup>a</sup>	35.0	0.05	10	120	3	1.2	70	37.8	1.08
Seymour-Johnson AFB <sup>a</sup>	30.9	0.05	4	120	3	1.2	70–75	29.2	0.94
New River <sup>a</sup>	47.4	0.05	10	120	3	1.2	70–75	40.2	0.85
Beaufort Marine Laboratory, N.C.	37.7	0.03	7	3,600	3	1.2	70–75	39.3	1.04
Opal (1995)									
Pensacola LLWSAS, Fla.	30.2	0.2, 0.05	12.2	600	3	0.9	30–40	41.7	1.38
Hurlburt Field <sup>a</sup>	54.3	0.01	3.5	120	3	0.9	30–40	59.5	1.10
Erin (1995)									
Pensacola LLWSAS	38.3	0.2, 0.05	12.2	600	3	1.7	42	39.2	1.02
Hurlburt Field <sup>a</sup>	49.6	0.01	3.5	120	3	1.7	42	48.4	0.98
Bob (1991)									
Providence Airport, R.I.	30.1	0.03	6.2	600	3	0.8	55–70	34.5	1.15
Logan Airport, Mass.	30.8	0.03	5.9	600	3	0.8	55–70	32.7	1.06
Hugo (1989)									
Myrtle Beach AFB, S.C.	40.5	0.03	3.0	900	3	1.0	40	37.1	0.92
Shaw AFB	55.0	0.05	4.6	900	3	1.0	40	54.8	1.00
Charleston Naval Station, S.C.	48.1	0.20	36.0	900	3	1.0	40	47.2	0.98
Charlotte Airport, N.C.	38.4	0.10	10.0	600	3	1.0	49	41.5	1.08
Columbia Airport, S.C.	33.5	0.05	6.1	600	3	1.0	40	38.2	1.14
Elena (1985)									
Mobile Airport, Ala.	28.2	0.05	6.7	600	3	1.55	22	33.2	1.18
Pensacola NAS, Fla.	32.3	0.10	23.8	600	3	1.55	22	34.2	1.06
Pensacola Airport, Fla.	30.4	0.05	6.7	600	3	1.55	22	30.6	1.01
Alicia (1983)									
Houston Airport, Tex.	36.8	0.05	6.1	600	3	1.2	55	44.8	1.22
Alvin WSO, Tex.	31.9	0.20	10.0	600	3	1.2	41–55	36.6	1.15
Galveston WSO, Tex.	36.2	0.30	32.0	600	3	1.2	41–55	38.1	1.05
Dow Plant "A," Tex.	38.2	0.15	10.0	600	3	1.2	28–55	35.9	0.94
Frederic (1979)									
Ingalls Shipyard, Miss.	50.4	0.05	10.0	600	3	1.3	38	52.0	1.03
Mobile Airport	45.2	0.05	6.7	600	3	1.3	38	49.0	1.08
Pensacola NAS	36.7	0.10	23.8	600	3	1.3	38	34.7	0.95
Pensacola Airport	36.7	0.05	6.7	600	3	1.3	38	33.1	0.90

Note: ASOS = Automated Surface Observing System; CF = Center Field; NAS = National Aerospace System; WSO = Weather Service Office.

<sup>a</sup>Stations record maximum in storm but are not continuous.

occurrence of a higher than average value of  $C_G$  at the peak of the storm. In general, the agreement between the simulated and observed wind speeds is good, particularly for winds approaching from easterly directions, where the upstream fetch is open. In the Dauphin Island case, the agreement between the simulated and observed peak gusts is generally good. The gust factors, however, appear to be consistently higher than the estimated values, particularly at the end of the record where a large change in wind direction is observed, suggesting the surface roughness may be larger than that assumed in the simulation.

Comparisons of the over land wind speeds are given in Fig. 5. In the over land comparisons, the overall characteristics of the hurricane, including  $R_{max}$ ,  $\Delta p$ , and position, are not as well known as in the over water and coastal cases because the NOAA aircraft flights are generally discontinued after a storm makes landfall. Overall the comparisons indicate the model

tends to slightly overestimate the inland wind speeds. Large overestimates are consistently seen in the Mobile, Ala., comparisons obtained in Hurricanes Frederic and Elena. In the Shaw Air Force Base (AFB), S.C., comparisons, the agreement between the simulated and observed peak wind speed occurs coincidentally with the occurrence of a large gust factor in the full-scale data. In the Charlotte, N.C., case, the observed gust factors are consistently higher than the simulated gust factors, with the overall agreement between the simulated and observed wind speeds being reasonable because the modeled mean wind speed is larger than the observed mean wind speed. For most of the inland stations examined, the far field is generally forested, and the extent to which this very rough far field influences the flow field at the anemometer site is unknown. These effects may be partly responsible for some of the lower mean wind speeds and higher gust factors observed at some locations. Considering the significant uncertainties as-

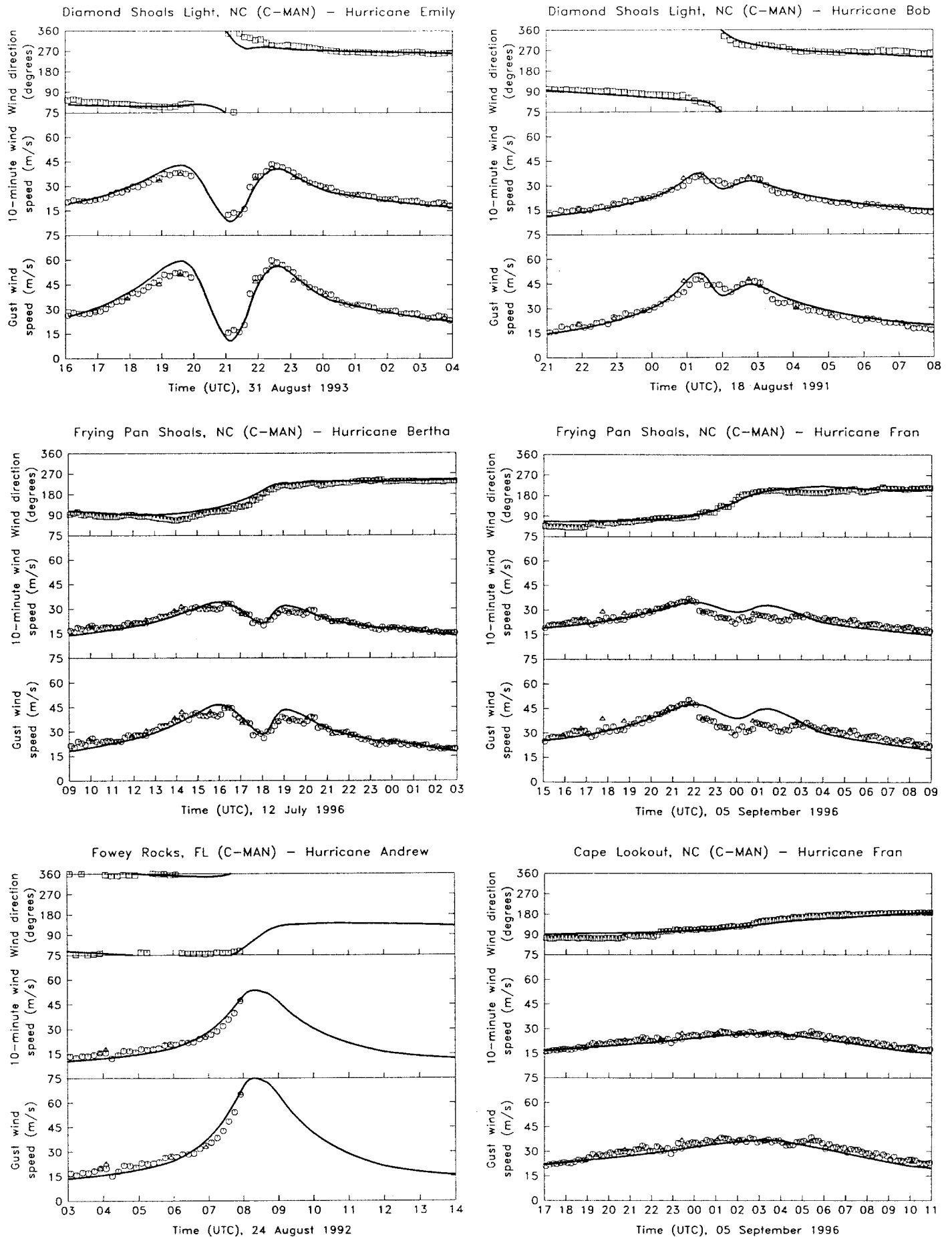


FIG. 3. Comparison of Simulated and Observed Wind Speeds for Marine Stations



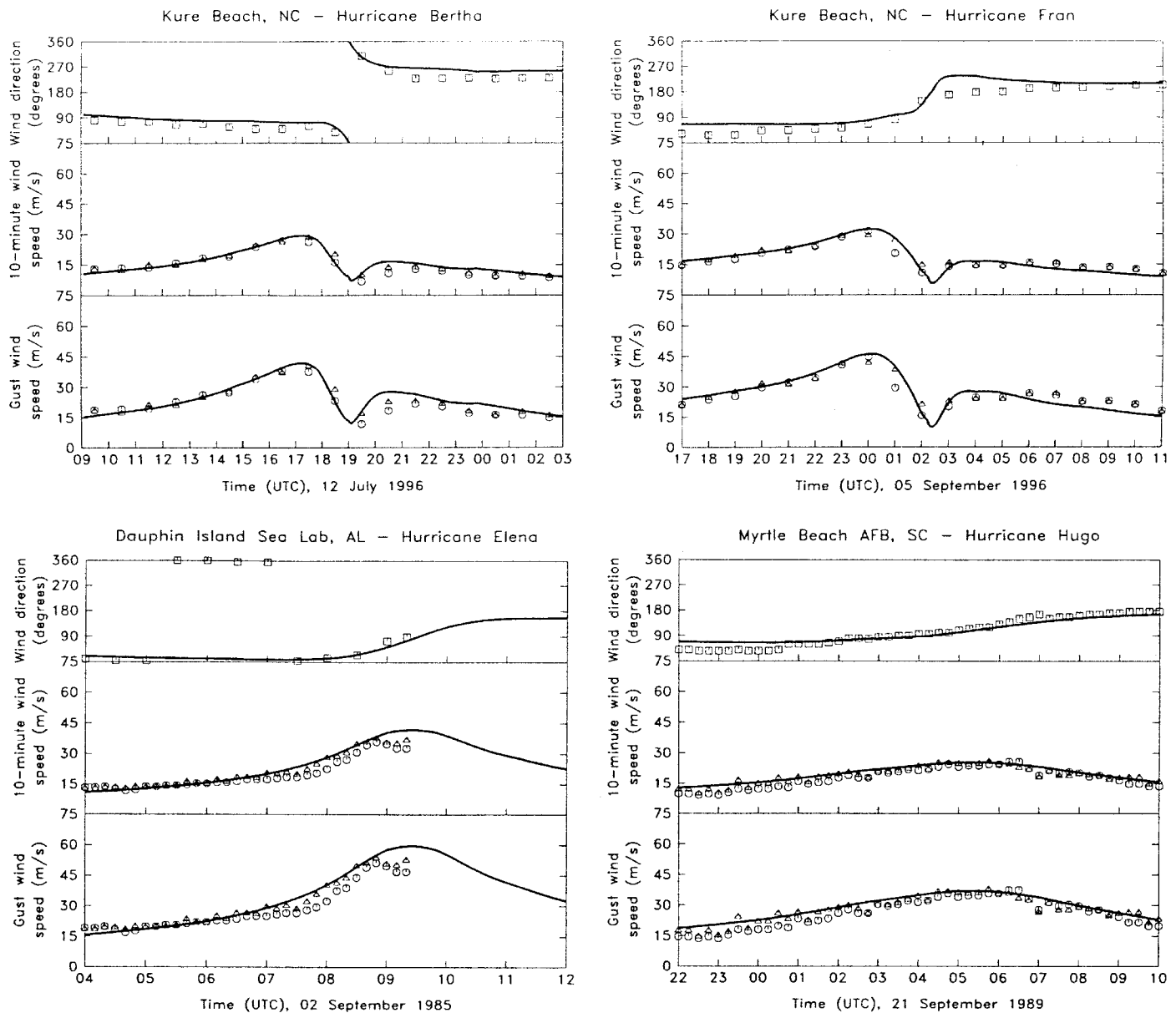


FIG. 4. Comparison of Simulated and Observed Hurricane Wind Speeds for Coastal Stations

sociated with the estimate of the local roughness and the far field roughness effects, the agreement between the observed and simulated wind speeds is considered good.

### Anomalous Wind Speed Comparisons

Fig. 6 shows some example cases where the comparisons between the simulated and observed wind speeds are poor and/or when features of the storm cannot be modeled using the hurricane wind field model. In the case of the low level wind alert system (LLWAS) comparisons for Hurricane Opal, the wind field model consistently overestimates the measured wind speeds and, in the Hurlburt Field, Fla., comparisons, a significant overestimate is evident after about 2250 on October 4. The poor agreement in these two cases is attributed to the complex interaction between the hurricane and a frontal system at the time of landfall, coupled with an eye-wall replacement that also was taking place at the time of landfall. The details of this complex interaction are given in Powell and Houston (1998).

In the Hurricane Bertha wind speed comparisons taken from the Cape Lookout C-MAN (CLKN7), the underestimate of the

wind speeds between 1600 and 1900 is associated with a large rain band, which is evident in the Doppler radar data given in Houston et al. (1997). Fig. 6 shows that the rain band influences both the mean and the peak wind speeds to approximately the same degree as indicated by the lack of anomalous gust factors during the 3 h. The higher wind speeds associated with rain bands away from the eye wall are features that cannot be modeled using a traditional pressure-driven wind field model.

### Effect of Parameters $B$ and $R_{max}$ on Wind Speed Comparisons

The comparisons of the simulated and observed wind speeds are influenced by the estimates of the full-scale parameters, including central pressure, position, radius to maximum winds, and the estimate of Holland's  $B$  parameter. Errors in the estimate of the central pressure are considered to be small and are not examined. Errors in the position of the storm appear in two ways. Position errors along the track of the storm appear as time shifts in the comparison of simulated and observed wind speeds. Position errors perpendicular to the direction of

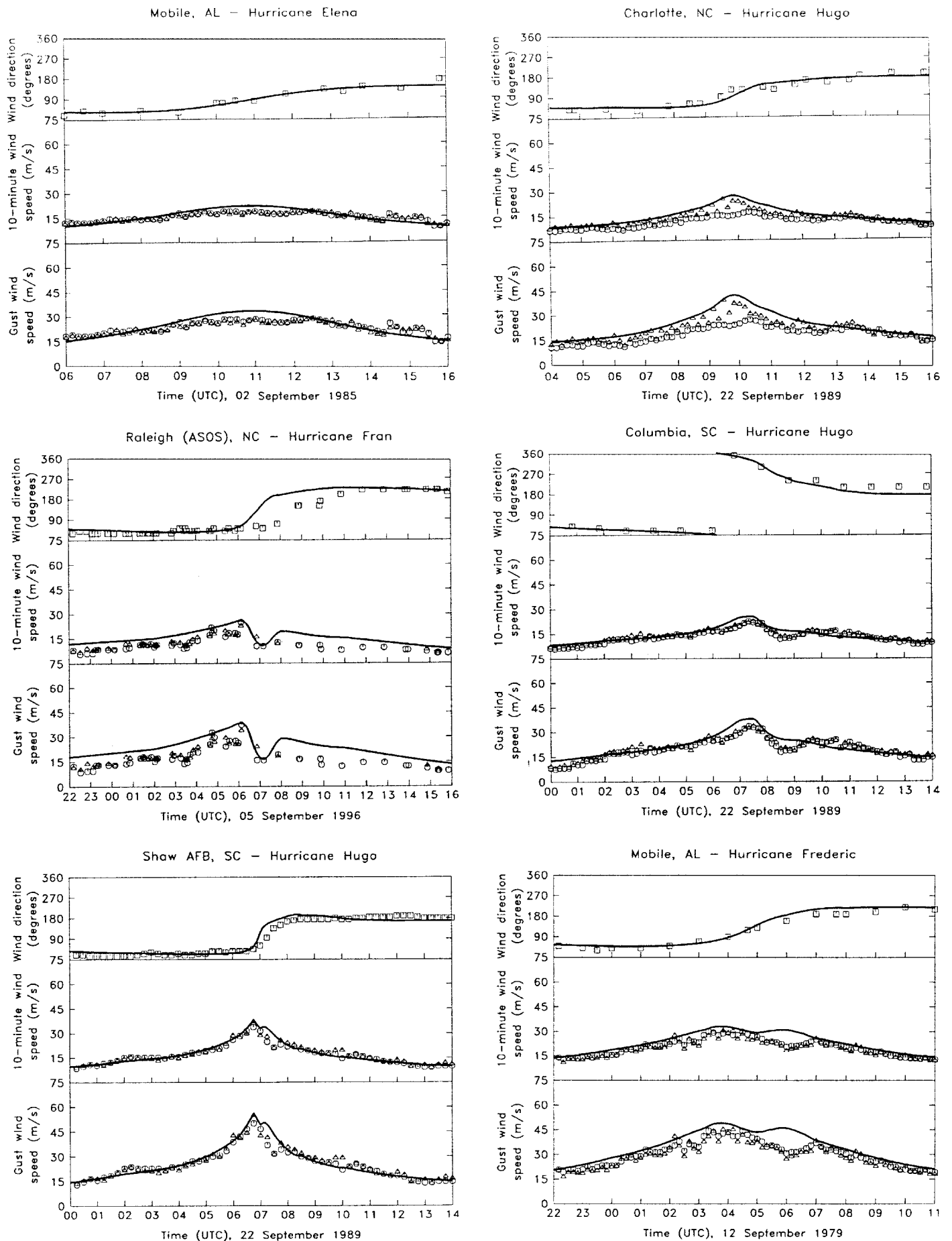


FIG. 5. Comparison of Simulated and Observed Hurricane Wind Speeds for Land Stations

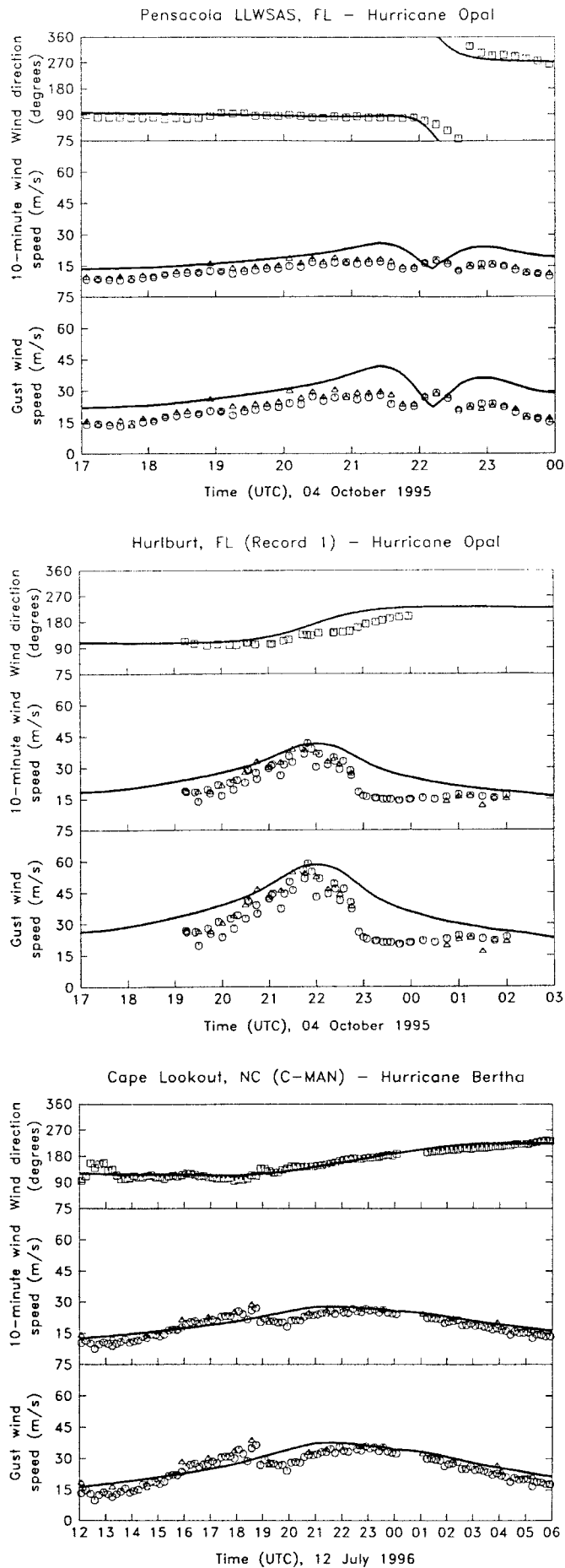


FIG. 6. Anomalous Wind Speed Comparisons

the storm have an effect similar to errors in the radius to maximum winds, effectively moving the station either closer to the storm center or further away from the storm center. The effect of  $R_{\max}$  and  $B$  on the wind speed comparisons is examined briefly here as these two parameters are the most difficult to measure, requiring a separate analysis of upper-level wind speed data obtained from NOAA aircraft. Furthermore, these parameters often vary over the domain of the storm and can change during the time the aircraft are performing the wind speed measurements.

Fig. 7 shows the effect of changing  $R_{\max}$  by  $\pm 20\%$  about the values given in Tables 1 and 2. As seen in Fig. 7, changing  $R_{\max}$  has little effect on the maximum wind speed at the station (typically  $< 5\%$ ) and has virtually no effect on the wind direction. On a point-by-point basis, the effect of changes in  $R_{\max}$  varies, depending upon the relative position of the station with respect to the center of the storm. For stations well removed from  $R_{\max}$  (not shown), increasing  $R_{\max}$  results in an increase in the simulated wind speeds; however, these lower wind speeds typically do not contribute significantly to the wind speeds associated with design-level events. For example, in the case of the next-generation water level measuring site (NGWLMS) at Haulover Pier, Fla., measurements taken during Hurricane Andrew, a 20% increase in the radius to maximize winds yields a 9% increase in the simulated peak gust wind speed, but this station is located at a distance of  $2.6R_{\max}$  to the right of the storm's center.

Fig. 8 shows the effect of changing  $B$  by  $\pm 20\%$  about the values given in Tables 1 and 2. Note that an increase in  $B$  results in an increase in the maximum storm wind speed. As indicated in Fig. 8, changing  $B$  does have an effect on the simulated maximum wind speed at each station with the impact varying with the relative position of the station with respect to the storm center and the initial value of  $B$ . The change in the maximum wind speed was seen to vary by as much as 17% in the case of the Hurricane Emily comparison to as little as about 5% in the case of the Shaw AFB comparison, with the greatest impact always occurring near  $R_{\max}$ .

In general, errors in the estimation of  $R_{\max}$  have the greatest impact on locations well removed from the center of the storm ( $r > 2R_{\max}$ ) and errors in the parameter  $B$  have the greatest impact on locations located within about  $2R_{\max}$  of the center of the storm.

### Hurricane Bertha's Wind Field on July 12, 1996, 1930

Another means to validate a hurricane wind field model is to compare the spatial distribution of simulated wind speed with the wind fields routinely constructed by HRD/NOAA. The HRD constructs surface wind fields at various stages throughout hurricanes by using all available wind speed observations within the domain of the storm. Observations may come from ships, buoys, coastal platforms, airports, reconnaissance aircraft, and other anemometer sites. Powell et al. (1996) described the methodology used for HRD's surface wind field analyses as it pertains to the reconstruction of Hurricane Andrew's wind field. Powell et al. (1996) assessed a 7% uncertainty associated with the procedures used to convert oceanic wind speed observations to 1-min peak values at a height of 10 m. They also estimated a 20% uncertainty associated with standardizing the upper-level wind speeds reported by the reconnaissance aircraft to surface-level wind speeds at 10 m.

To further validate the hurricane wind field model, the simulated wind field of Hurricane Bertha at about 20 min prior to landfall is compared to HRD's constructed wind field for the same time. The HRD performed 16 wind field analyses for Hurricane Bertha. Houston et al. (1997) documented the analysis of the surface wind field for Hurricane Bertha at the time

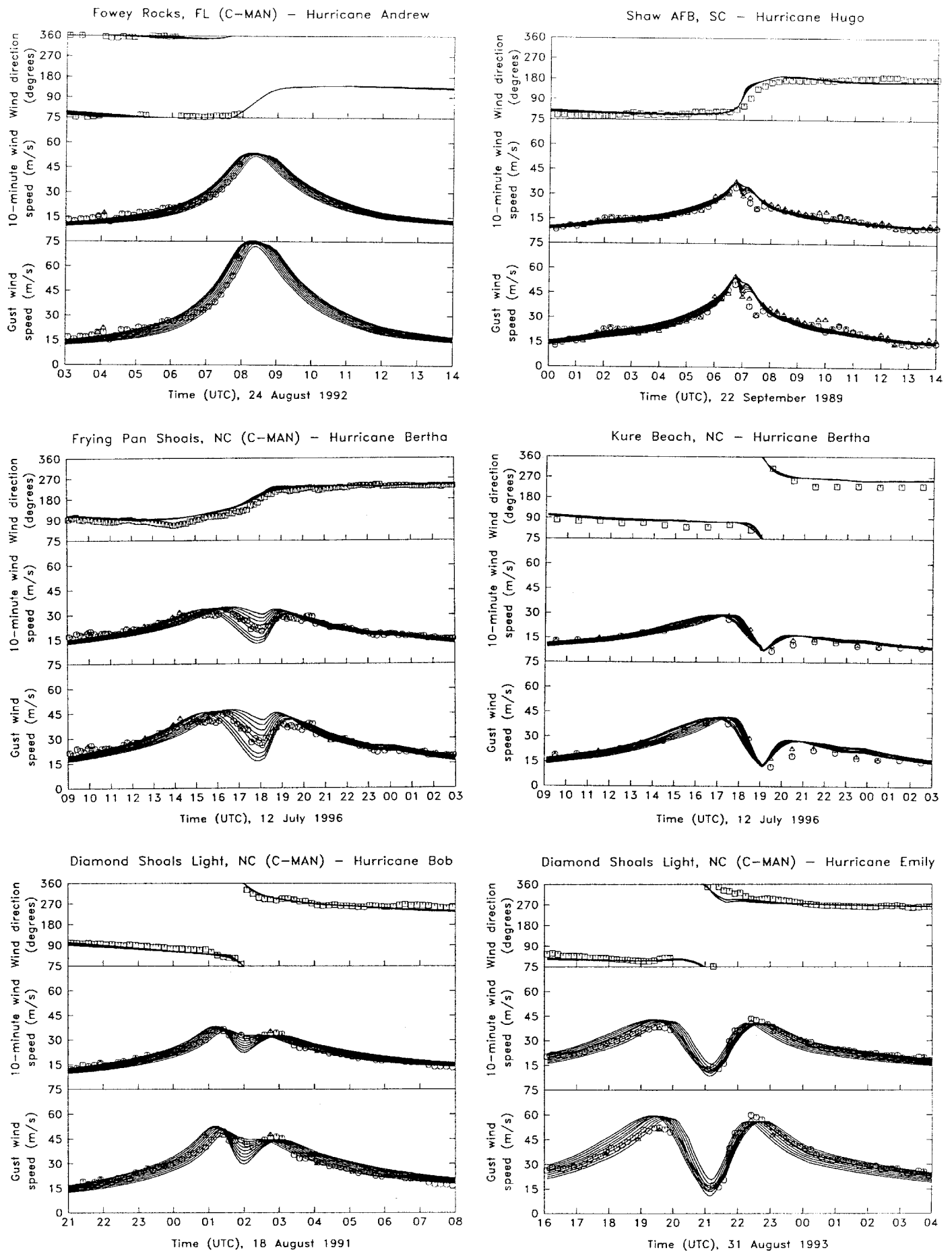


FIG. 7. Effect of Changes in Radius to Maximum Winds on Wind Speed Comparisons

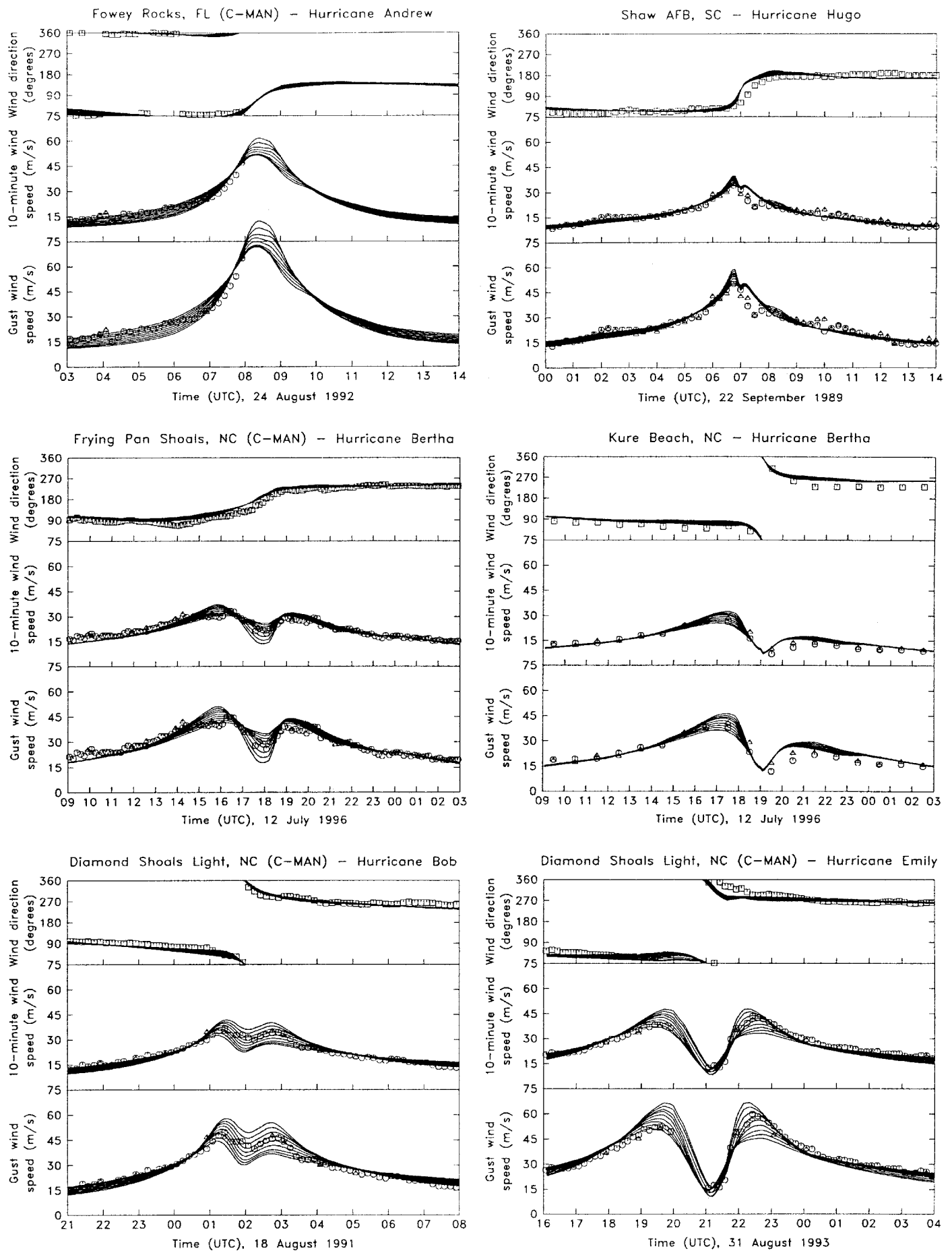


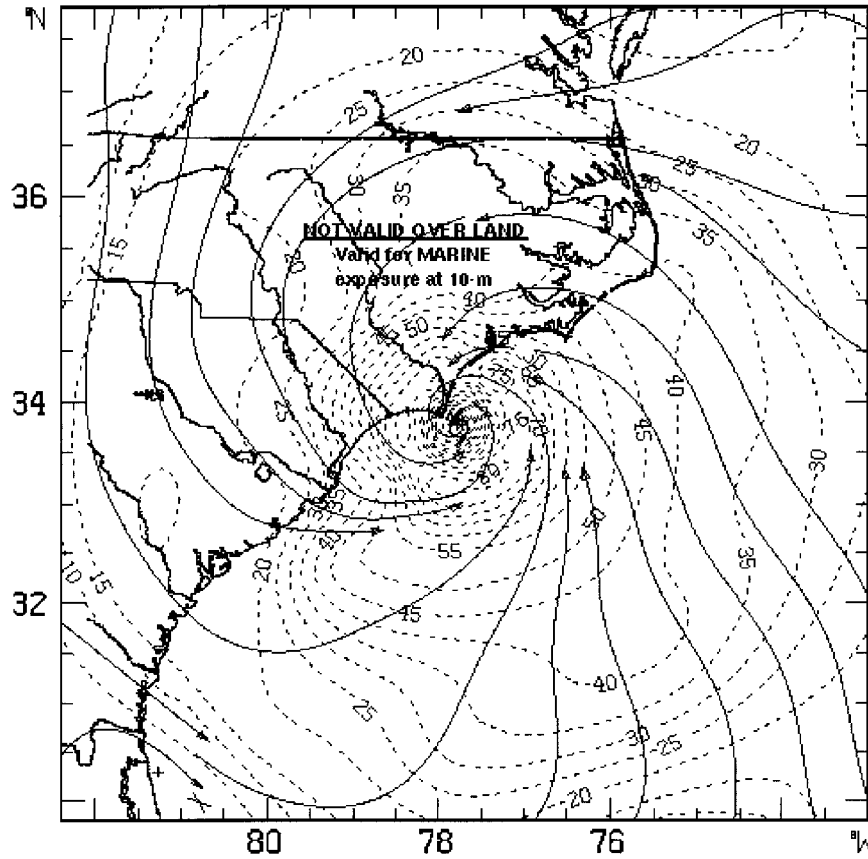
FIG. 8. Effect of Changes in Holland's  $B$  Parameter on Wind Speed Comparisons

# Hurricane Bertha 1930 UTC 12 Jul. 1996

## Maximum sustained 1-min surface winds

Streamlines and Isotachs (kt) using

Air Force Reserve recon. data adjusted to the surface from  
700 mb during 1530 - 1748 z and marine sfc. observations from 1400 - 1800 z  
1930 z position extrapolated from the 1712 z fix using 11 kt @ 15°



Experimental research product of:

**NOAA / AOML / Hurricane Research Division**

FIG. 9. HRD Wind Field for Hurricane Bertha—Maximum Sustained Surface Winds (Knots), from HRD's Web Site: <http://www.aoml.noaa.gov/hrd>

TABLE 3. Percentage Error in Simulated versus Observed 10-min Mean Wind Speeds

Station type (1)	Gust wind speed range (m/s) (2)	$ r/R_{max}  \leq 2$					$2 <  r/R_{max}  \leq 4$				
		Sample size (3)	Mean (4)	Standard deviation (5)	Maximum (6)	Minimum (7)	Sample size (8)	Mean (9)	Standard deviation (10)	Maximum (11)	Minimum (12)
Marine	$15 \leq V < 25$	1	16.20	—	16.20	16.20	57	-3.04	16.59	54.10	-26.43
	$25 \leq V < 35$	11	4.58	10.56	20.25	-14.10	56	-5.37	8.86	15.49	-22.29
	$35 \leq V < 45$	23	4.05	9.88	26.26	-13.78	6	-9.16	11.17	-1.35	-29.43
	$V \geq 45$	11	-0.11	8.52	11.38	-15.86	0	—	—	—	—
	$V_{max} \geq 35$	6	-0.72	3.69	2.70	-5.92	1	-23.28	—	-23.28	-23.28
Coastal	$15 \leq V < 25$	24	-0.38	31.80	96.35	-37.29	60	10.40	19.25	52.96	-16.67
	$25 \leq V < 35$	43	9.25	16.16	49.69	-14.59	29	10.96	10.44	27.93	-5.90
	$35 \leq V < 45$	25	17.63	11.42	36.03	-7.85	1	28.87	—	28.87	28.87
	$V \geq 45$	9	12.65	9.81	27.51	-2.14	0	—	—	—	—
	$V_{max} \geq 35$	4	4.02	4.05	9.33	-0.48	0	—	—	—	—
Land	$15 \leq V < 25$	105	27.19	23.97	93.64	-46.18	217	21.25	15.02	59.42	-21.58
	$25 \leq V < 35$	169	21.16	15.22	84.42	-35.84	202	9.90	10.30	37.14	-14.16
	$35 \leq V < 45$	35	17.77	19.65	81.13	1.88	14	-1.16	6.60	13.43	-11.28
	$V \geq 45$	3	13.62	3.96	16.72	9.16	0	—	—	—	—
	$V_{max} \geq 35$	10	12.42	19.34	59.39	-10.56	3	-0.62	11.72	12.84	-8.53

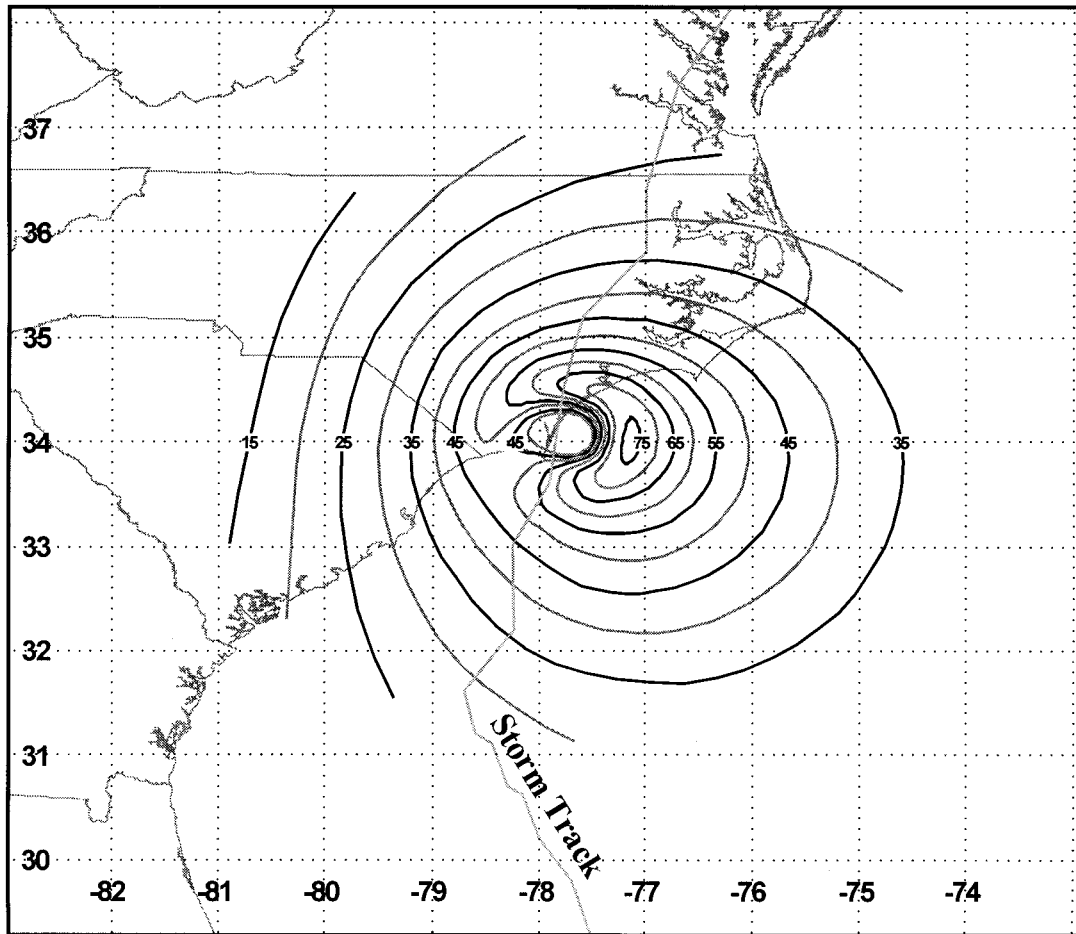


FIG. 10. Simulated Wind Field—Hurricane Bertha 1930 UTC July 12, 1996—Maximum Sustained Surface Wind Speeds (Knots) at 10 m for Marine Exposure

TABLE 4. Percentage Error in Simulated versus Observed Gust Wind Speeds

Station type (1)	Gust wind speed range (m/s) (2)	$ r/R_{\max}  \leq 2$					$2 <  r/R_{\max}  \leq 4$				
		Sample size (3)	Mean (4)	Standard deviation (5)	Maximum (6)	Minimum (7)	Sample size (8)	Mean (9)	Standard deviation (10)	Maximum (11)	Minimum (12)
Marine	$15 \leq V < 25$	1	7.97	—	7.97	7.97	57	-5.27	11.37	28.87	-26.59
	$25 \leq V < 35$	12	2.38	11.23	25.02	-17.21	56	-7.00	10.80	23.18	-37.17
	$35 \leq V < 45$	23	3.21	10.30	26.39	-13.20	6	-16.77	10.89	-2.39	-31.96
	$V \geq 45$	11	2.34	9.33	17.53	-12.04	0	—	—	—	—
	$V_{\max} \geq 35$	6	1.69	4.25	8.01	-2.67	1	-24.62	—	-24.62	-24.62
Coastal	$15 \leq V < 25$	24	0.89	21.04	47.08	-32.29	60	9.50	14.36	45.60	-31.97
	$25 \leq V < 35$	43	9.48	14.72	47.78	-20.69	29	3.33	7.12	18.31	-11.14
	$35 \leq V < 45$	25	7.50	6.85	21.32	-3.64	1	6.24	—	6.24	6.24
	$V \geq 45$	9	3.95	10.57	17.38	-18.16	0	—	—	—	—
	$V_{\max} \geq 35$	4	5.32	3.37	10.31	3.22	0	—	—	—	—
Land	$15 \leq V < 25$	105	26.09	23.19	84.18	-50.29	217	19.47	12.97	54.82	-19.61
	$25 \leq V < 35$	169	19.09	13.87	69.37	-37.72	202	5.98	9.15	30.58	-21.06
	$35 \leq V < 45$	35	11.38	10.11	29.51	-7.81	14	-5.82	3.18	-0.67	-12.17
	$V \geq 45$	3	4.46	4.79	8.34	-0.89	0	—	—	—	—
	$V_{\max} \geq 35$	10	4.12	10.19	21.81	-16.90	3	-7.86	2.27	-5.40	-9.88

of landfall. The HRD's wind field for Hurricane Bertha on July 12, 1996, at 1930, about 20 min prior to landfall, is shown in Fig. 9. Fig. 10 shows the simulated wind field for Hurricane Bertha at the same time. The isotachs on both of the plots represent peak sustained (1-min mean) wind speeds at 10 m for a marine exposure.

The HRD's wind field analysis shows peak sustained wind speeds >80 knots (41.2 m/s) located approximately south-southeast of the storm's center. This can be compared to the

simulated wind field, which produces peak sustained wind speeds of about 76 knots (39.1 m/s) east of the storm's center. The storm size comparison is made by considering the areas enclosed by the 35-knot (18.0-m/s) and 45-knot (23.2-m/s) isotachs. The area enclosed by the outer 35-knot (18.0-m/s) isotach of the simulated wind field matches well with that of the HRD wind field for the sector approximately between west-southwest through west to northwest and for small sectors toward the east-southeast and toward the northeast. For

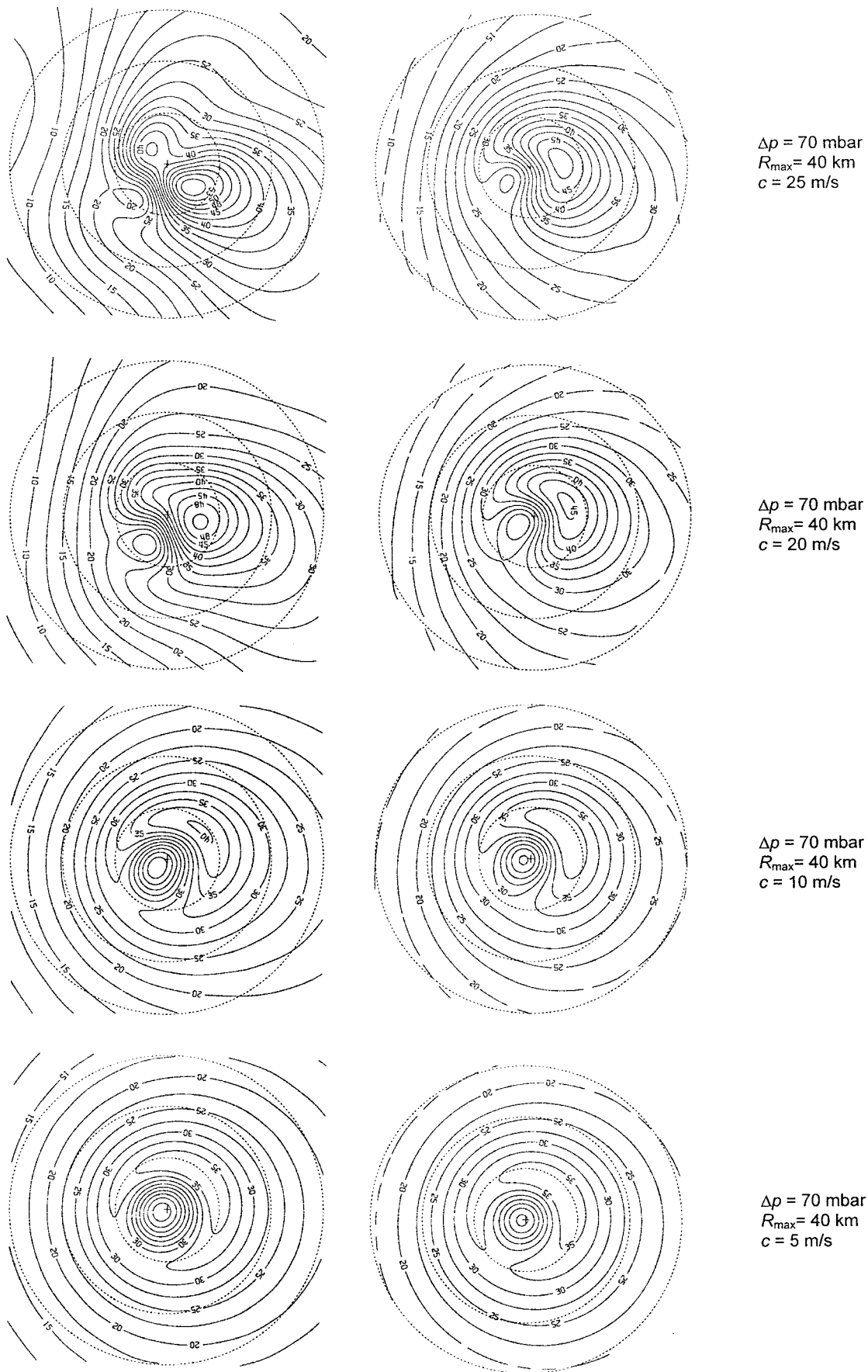


**FIG. 11. Isotachs of 1-h Mean Wind Speed (Meters per Second) over Open Terrain at 10 m above Ground: Key Hurricane Properties Are  $R_{max} = 40$  km,  $\Delta p = 70$  mbar,  $B = 1.4$ , Air-Sea Temperature Difference =  $0^{\circ}\text{C}$ , Translation Speed  $c$  Varies as Indicated; Hurricanes Are Moving toward Top of Page; Plots on Left-Hand Side of Page Are Derived from Shapiro-Based Wind Field Model Used by Vickery and Twisdale (1995a); Plots on Right-Hand Side of Page Are Derived from Wind Field Model Described Herein**



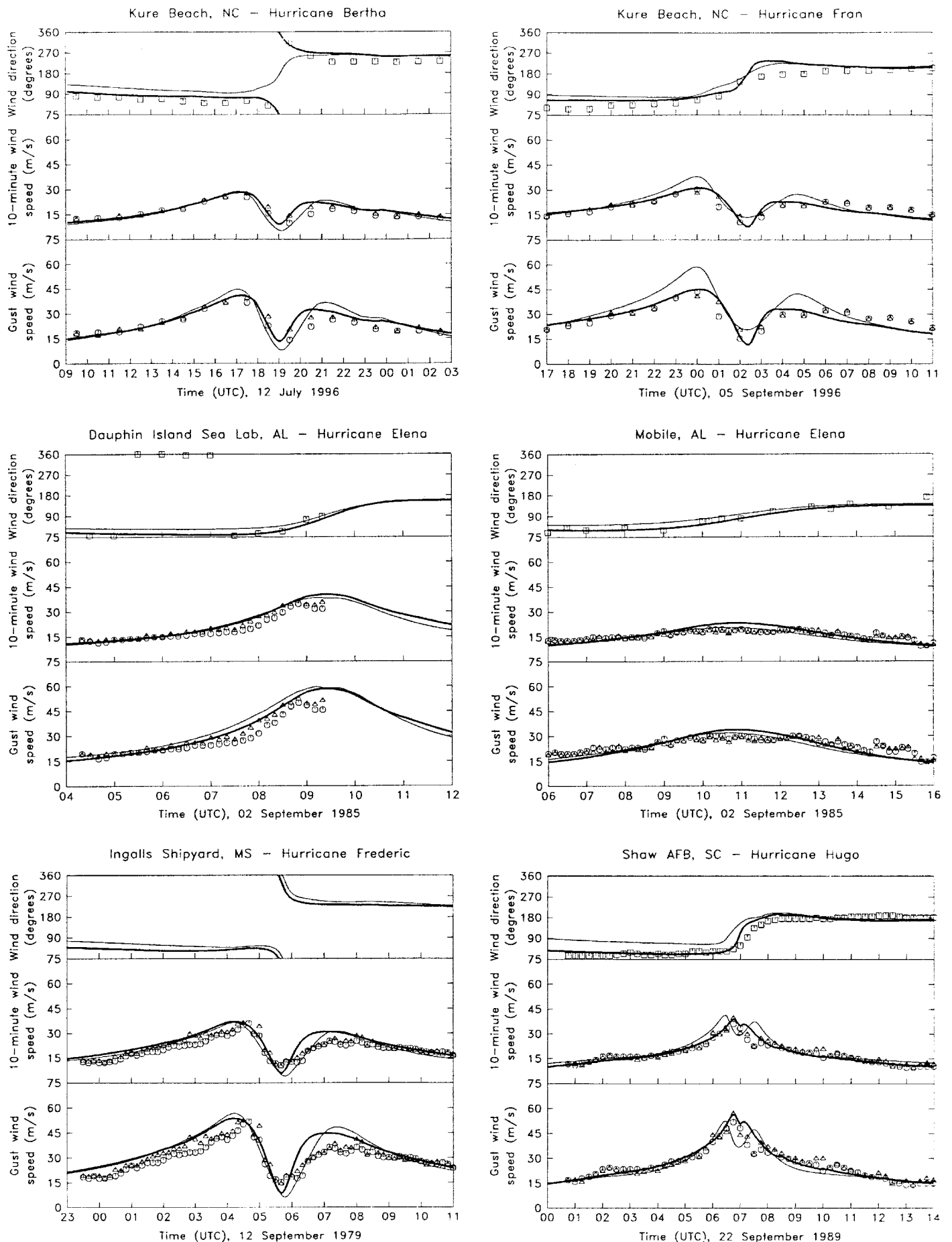


**FIG. 12. Comparison of Simulated and Observed Hurricane Wind Speeds over Open Terrain at 10 m above Ground [Thin Solid Lines Are Derived from Shapiro-Based Wind Field Model Used by Vickery and Twisdale (1995a); Thick Solid Lines Are Derived from Wind Field Model Described Herein; Points Are Observed Wind Data]**

the remaining directional sectors, the simulated wind field yields smaller radial distances to the outer 35-knot (18.0-m/s) isotach (typically about 90-km smaller) than does the HRD wind field analyses (i.e., the simulated wind field is tighter). A comparison of the radial extent of the outer 45-knot (23.2-m/s) isotach shows a good match for the sector roughly between west-southwest through north to east. The simulated wind field, however, yields a smaller area with peak sustained wind speeds >45 knots (23.2-m/s) for the remaining directional sector (i.e., west-southwest through south to east). Within this region, the radial distance to the 45-knot (23.2-m/s) isotach is up to about 140 km shorter in the simulated wind field compared to the HRD's wind field.

The performance of the wind field model on matching the storm size is considered good, given that the model uses only one value of the radius to maximum winds and only one value of the Holland pressure profile parameter for all directional sectors. In reality, a hurricane interacts with large-scale atmospheric flows and there can be significant directional variations in storm size and pressure distribution. This was observed when analyzing 1,300 radial profiles of wind speed and pressure measured by reconnaissance aircraft in 27 different hurricanes. For example, between 0959 and 1039 on September 1, 1985, an analysis of the upper-level wind speed data measured during Hurricane Elena yields estimates of  $R_{\max}$  and  $B$  equal to 38 km and 1.53, respectively, east of the storm's center and 30 km and 1.28, respectively, west of the storm center (Vickery et al. 2000).

## Error Analysis

Tables 3 and 4 present a summary of the percent differences between the simulated and observed 10-min mean and peak gust wind speeds, both as a function of gust wind speed range. Note that the wind speed ranges given in each table are based on the observed gust wind speed. The percent differences are computed as  $100 \cdot (\text{simulated} - \text{observed}) / \text{observed}$ . The comparisons in the main body of the table are made over the entire duration of the wind speed traces and not simply the peak value observed. A comparison of the single maximum wind speed value observed during the storm at each anemometer site is given at the bottom of each table for those cases where the maximum gust wind speed equaled or exceeded 35 m/s.

## COMPARISONS TO WIND FIELD MODEL USED IN VICKERY AND TWISDALE (1995a)

As indicated earlier, one of the main reasons for implementing the full solution of the equations of motion for a hurricane, rather than the two-term spectral model used in the Shapiro-based model employed by Vickery and Twisdale (1995a), was to better model the wind field in fast-moving hurricanes. Fig. 11 shows 1-h mean surface-level wind speeds as a function of storm translation speed. The full numerical solution results are given for a Holland pressure profile parameter equal to 1.4 and an air-sea temperature difference equal to zero. A comparison of the two sets of results indicates that at low translation speeds ( $c < 10$  m/s), the wind fields obtained using the two approaches are similar. However, using the spectral model (left-hand plots), the peak surface winds increase more rapidly with storm translation speed than do those modeled with the full solution. The comparisons also indicate that as the translation speed increases, the spectral-solution results become more asymmetric than the full-solution results, with the larger wind speeds extending much further to the right of the storm center. No full-scale wind speed data were available from fast-moving storms to determine which model provides a better representation of the wind field but, because the full numerical solution is better able to model the asymmetries, it

is believed that this model should yield a better representation of the wind field in fast-moving storms.

Fig. 12 shows surface wind speeds in open terrain conditions ( $z_0 = 0.03$  m) at a height of 10 m. The plots compare measured wind directions, peak gusts, and 10-min mean wind speeds to those estimated using the wind field model given in Vickery and Twisdale (1995a), which uses the gust factor curve given by Krayner and Marshall (1992), and those estimated with the wind field model described herein. In the examples presented in Fig. 12, the peak gust wind speeds produced by the model given in Vickery and Twisdale (1995a), in most cases, tend to be slightly higher than those produced by the new model, but overall the agreement is reasonable. The wind directions are clearly better modeled using the wind field model described in this paper.

In the case of the Kure Beach measurement taken during Hurricane Fran, the wind field model used by Vickery and Twisdale (1995a) overestimates the peak wind speeds. Noting that larger  $B$  values lead to higher wind speeds with all else being equal, these overestimates are brought about because, as indicated in Fig. 11, the wind field model in Vickery and Twisdale (1995a) appears to reproduce a wind field associated with a  $B$  value in the range of 1.3–1.5 and Hurricane Fran is modeled with a  $B$  value near unity. As indicated in Vickery et al. (2000), the mean value of  $B$  for Atlantic hurricanes is about 1.3; thus, on average the use of the Shapiro-based wind field model employed by Vickery and Twisdale (1995a,b) should yield reasonable estimates of predicted surface level wind speeds versus return period.

## SUMMARY AND CONCLUSIONS

The boundary layer modeling has been improved over the models used in prior hurricane risk studies by taking into account the air-sea temperature difference and the change in the sea surface roughness with wind speed. Also, use is made of a physically based gust factor model that properly models the variation in the gust factor with surface roughness.

The modeling of the hurricane wind field also has been improved in comparison to models used in previous studies, employing the full nonlinear solution to the equations of motion of a hurricane rather than the spectral model used in Georgiou (1985) or Vickery and Twisdale (1995a) or the empirical models used in all other studies. Evaluation of the hurricane model through comparisons with real hurricane wind speed data show that the model provides a good representation of the hurricane wind field, provided reasonable estimates of  $B$  and  $R_{\max}$  are available. Considering that in most real hurricanes, both the pressure profile parameter and the radius to maximum winds vary both spatially and temporally, the observed agreement between simulated and observed storms is good.

## ACKNOWLEDGMENTS

The research described in this paper was partly supported by the National Science Foundation, Washington, D.C., under a Phase II Small Business Innovation Research Grant, ISI 9304222, and the National Association of Home Builders, Washington, D.C.

The results, findings and conclusions of this study are those of the writers and do not represent those of the sponsors.

## APPENDIX. REFERENCES

- Arya, S. P. S. (1998). *Introduction to micrometeorology*, Chapter 11, Academic, San Diego.
- Batts, M. E., Cordes, M. R., Russell, L. R., Shaver, J. R., and Simiu, E. (1980). "Hurricane wind speeds in the United States." *Rep. No. BSS-124*, Nat. Bureau of Standards, U.S. Department of Commerce, Washington, D.C.
- Burpee, R. W., et al. (1994). "Real-time guidance provided by NOAA's Hurricane Research Division to forecasters during Emily of 1993." *Bull. Am. Meteorological Soc.*, 75(10), 1765–1783.
- Chow, S. H. (1971). "A study of windfield in the planetary boundary

- layer of a moving tropical cyclone." MS thesis, School of Engrg. and Sci., New York University, New York.
- Deaves, D. M. (1981). "Terrain-dependence of longitudinal R.M.S. velocities in the neutral atmosphere." *J. Wind Engrg. and Industrial Aerodynamics*, Amsterdam, The Netherlands, 8, 259–274.
- Georgiou, P. N. (1985). "Design windspeeds in tropical cyclone-prone regions." PhD thesis, Fac. of Engrg. Sci., University of Western Ontario, London, Ont., Canada.
- Georgiou, P. N., Davenport, A. G., and Vickery, B. J. (1983). "Design wind speeds in regions dominated by tropical cyclones." *J. Wind Engrg. and Industrial Aerodynamics*, Amsterdam, The Netherlands, 13(1), 139–152.
- Golden, J. H. (1984). "Meteorological overview of Hurricane Alicia." *Proc., ASCE Spec. Conf.: Alicia, One Year Later*, ASCE, New York, 1–20.
- Ho, F. P., Su, J. C., Hanevich, K. L., Smith, R. J., and Richards, F. P. (1987). "Hurricane climatology for the Atlantic and Gulf coasts of the United States." *NOAA Tech. Rep. NWS38*, Federal Emergency Management Agency, Washington, D.C.
- Hock, T. F., and Franklin, J. L. (1999). "The NCAR GPS dropwindsonde." *Bull. Am. Meteorological Soc.*, 80(3), 407–420.
- Holland, G. J. (1980). "An analytic model of the wind and pressure profiles in hurricanes." *Monthly Weather Rev.*, 108(8), 1212–1218.
- Houston, S. H., and Powell, M. D. (1993). "Surface wind fields during Hurricane Bob's (1991) landfall in New England." *Proc., 20th Conf. on Hurricanes and Tropical Meteorology*, American Meteorological Society, Boston, 139–142.
- Houston, S. H., Powell, M. D., and Dodge, P. P. (1997). "Surface wind fields in 1996 Hurricanes Bertha and Fran at landfall." *Proc., 22nd Conf. on Hurricanes and Tropical Meteorology*, American Meteorological Society, Boston, 92–93.
- Jarvinen, B. R., Neumann, C. J., and Davis, M. A. S. (1984). "A tropical cyclone data tape for the North Atlantic Basin 1886–1983: Contents, limitations and uses." *NOAA Tech. Memo. NWS NHC 22*, U.S. Department of Commerce, Washington, D.C.
- Krayer, W. R., and Marshall, R. D. (1992). "Gust factors applied to hurricane winds." *Bull. Am. Meteorological Soc.*, 73(5), 613–617.
- Powell, M. D. (1980). "Evaluations of diagnostic marine boundary-layer models applied to hurricanes." *Monthly Weather Rev.*, 108, 757–766.
- Powell, M. D., and Black, P. G. (1990). "The relationship of hurricane reconnaissance flight-level wind measurements to winds measured by NOAA's oceanic platforms." *J. Wind Engrg. and Industrial Aerodynamics*, Amsterdam, The Netherlands, Vol. 36, 381–392.
- Powell, M. D., Dodge, P. P., and Black, L. B. (1991). "The landfall of Hurricane Hugo in the Carolinas: Surface wind distribution." *Weather and Forecasting*, 6, 379–399.
- Powell, M. D., and Houston, S. H. (1998). "Surface wind fields of 1995 Hurricanes Erin, Opal, Luis, Marilyn, and Roxanne at landfall." *Monthly Weather Rev.*, 126(5), 1259–1273.
- Powell, M. D., Houston, S. H., and Reinhold, T. A. (1996). "Hurricane Andrew's landfall in South Florida—Part I: Standardizing measurements for documentations of surface wind fields." *Weather and Forecasting*, 11(3), 303–328.
- Powell, M. D., Reinhold, T. A., and Marshall, R. D. (1999). "GPS sonde insights on boundary layer structure in hurricanes." *Proc., 10th Int. Conf. on Wind Engrg.*, A. A. Balkema, Rotterdam, The Netherlands.
- Russell, L. R. (1971). "Probability distributions for hurricane effects." *J. Wtrwy., Harb. and Coast. Engrg. Div.*, ASCE, 97(1), 139–154.
- Shapiro, L. J. (1983). "The asymmetric boundary layer flow under a translating hurricane." *J. Atmospheric Sci.*, 40(8), 1984–1998.
- Smagorinsky, J. (1963). "General circulation experiments with the primitive equations—I. The basic experiment." *Monthly Weather Rev.*, 91(3), 99–164.
- "Strong winds in the atmospheric boundary layer, Part 1: Mean hourly wind speed." (1982). *Item No. 82026*, Engineering Sciences Data Unit, London.
- "Strong winds in the atmospheric boundary layer, Part 2: Discrete gust speeds." (1983). *Item No. 83045*, Engineering Sciences Data Unit, London.
- Thompson, E. F., and Cardone, V. J. (1996). "Practical modeling of hurricane surface wind fields." *J. Wtrwy., Port, Coast., and Oc. Engrg.*, ASCE, 122(4), 195–205.
- Vickery, P. J., Skerlj, P. F., and Twisdale, L. A. (2000). "Simulation of hurricane risk in the U.S. using empirical track model." *J. Struct. Engrg.*, ASCE, 126(10), 1222–1237.
- Vickery, P. J., and Twisdale, A. (1995a). "Wind-field and filling models for hurricane wind-speed predictions." *J. of Struct. Engrg.*, ASCE, 121(11), 1700–1709.
- Vickery, P. J., and Twisdale, A. (1995b). "Prediction of hurricane wind speeds in the United States." *J. Struct. Engrg.*, ASCE, 121(11), 1691–1699.
- Willoughby, H. B. (1990). "Gradient balance in tropical cyclones." *J. Atmospheric Sci.*, 47(2), 265–274.